JOURNAL OF GEOPHYSICAL RESEARCH, VOL. 117, D09304, doi:10.1029/2011JD017246, 2012

Precipitating radiation belt electrons and enhancements of mesospheric hydroxyl during 2004–2009

Monika E. Andersson,[1] Pekka T. Verronen,[1] Shuhui Wang,[2] Craig J. Rodger,[3] Mark A. Clilverd,[4] and Bonar R. Carson[3]

Received 30 November 2011; revised 3 April 2012; accepted 3 April 2012; published 10 May 2012.

[1] Energetic particle precipitation leads to enhancement of odd hydrogen (HO_x) below 80 km altitude through water cluster ion chemistry. Using measurements from the Microwave Limb Sounder (MLS/Aura) and Medium Energy Proton and Electron Detector (MEPED/POES) between 2004–2009, we study variations of nighttime OH caused by radiation belt electrons at geomagnetic latitudes 55–65°. For those months with daily mean 100–300 keV electron count rate exceeding 150 counts/s in the outer radiation belt, we find a strong correlation ($r \geq 0.6$) between OH mixing ratios at 70–78 km (0.046–0.015 hPa) and precipitating electrons. Correlations $r \geq 0.35$, corresponding to random chance probability $p \leq 5\%$, are observed down to52 km (0.681 hPa), while no clear correlation is observed at altitudes below. This suggests that the fluxes of ≥3 MeV electrons were not high enough to cause observable changes in OH mixing ratios. At 75 km, in about 34% of the 65 months analyzed we find a correlation $r \geq 0.35$. Although similar results are obtained for both hemispheres in general, in some cases the differences in atmospheric conditions make the OH response more difficult to detect in the South. Considering the latitude extent of electron forcing, we find clear effects on OH at magnetic latitudes 55–72°, while the lower latitudes are influenced much less. Because the time period 2004–2009 analyzed here coincided with an extended solar minimum, and the year 2009 was anomalously quiet, it is reasonable to assume that our results provide a lower-limit estimation of the importance of energetic electron precipitation at the latitudes considered.

Citation: Andersson, M. E., P. T. Verronen, S. Wang, C. J. Rodger, M. A. Clilverd, and B. R. Carson (2012), Precipitating radiation belt electrons and enhancements of mesospheric hydroxyl during 2004–2009, *J. Geophys. Res.*, *117*, D09304, doi:10.1029/2011JD017246.

1. Introduction

[2] The odd hydrogen family (HO_x = H + OH + HO_2), especially hydroxyl (OH), has significant implications for ozone (O_3) chemistry via participation in catalytic reaction cycles that destroy ozone, and in reactions between different forms of other ozone depleting compounds [*Bates and Nicolet*, 1950]. The presence of HO_x in the middle atmosphere is a consequence of water vapor (H_2O), methane (CH_4) and molecular hydrogen (H_2) transported from the troposphere. In the upper stratosphere, H_2O reacts with atomic oxygen from O_3 photodissociation by UV radiation:

$$H_2O + O(^1D) \rightarrow 2OH. \quad (1)$$

In the mesosphere, photodissociation of H_2O by absorption of UV radiation,

$$H_2O + h\nu \rightarrow OH + H, \quad (2)$$

produces OH and H and, consequently, leads to rapid decrease in water vapor mixing ratios especially above 80 km altitude [*Brasseur and Solomon*, 1986]. The main contributor to water vapor dissociation at altitudes above 68 km is the Lyman-α line (121.568 nm), whereas between 60–68 km the Schumann-Runge band region (175–200 nm) plays a major role [*Frederick and Hudson*, 1980]. Above 40 km, the destruction of odd hydrogen is controlled mainly through reactions with atomic oxygen and HO_x recombination [*Canty and Minschwaner*, 2002]. The chemical lifetime limit for HO_x at 75–80 km altitudes is between 0.1–1 day and increases up to 30 days at altitudes above 85 km [*Pickett et al.*, 2006]. Therefore, atmospheric transport of HO_x below 80 km is negligible. For OH, seasonal

[1]Earth Observation Unit, Finnish Meteorological Institute, Helsinki, Finland.
[2]Jet Propulsion Laboratory, California Institute of Technology, Pasadena, California, USA.
[3]Department of Physics, University of Otago, Dunedin, New Zealand.
[4]British Antarctic Survey, NERC, Cambridge, UK.

Corresponding author: M. E. Andersson, Earth Observation Unit, Finnish Meteorological Institute, Erik Palménin aukio 1, PO Box 503, Helsinki FI-00101, Finland. (monika.andersson@fmi.fi)

0148-0227/12/2011JD017246

Table 1. Data Characteristics[a]

Data	SEM_{day} NH/SH (%)	SEM_{month} NH/SH (%)	n_{min} NH/SH	n_{max} NH/SH
OH	7/16	8/6	11/43	115/198
H_2O	2/4	2/1	11/40	114/195
Temperature	0.2/0.3	0.4/0.3	11/43	115/197
I_α^{SZA}	–	3/5	–	–
ECR	26	42	–	–

[a]SEM_{day} = mean value of standard error of the daily mean. SEM_{month} = mean value of standard error of monthly mean. n_{min} and n_{max} are the typical minimum and maximum number of data profiles or points per day, respectively, available for average calculations. Note that the MLS numbers are given for the 75 km altitude and separately for the geomagnetic latitudes 55–65°N/S.

and solar cycle variability is connected to solar activity together with the seasonal variation of water vapor and ozone in the mesosphere [*Canty and Minschwaner*, 2002] whereas the diurnal variability of OH is related to the solar zenith angle (SZA) variation during the day and can be characterized by exponential functions of the secant of SZA [*Minschwaner et al.*, 2011].

[3] An important mechanism affecting the neutral chemistry of the atmosphere in the polar regions and resulting in the enhancement of odd hydrogen species is energetic particle precipitation [*Thorne*, 1977; *Heaps*, 1978; *Verronen et al.*, 2006, 2007; *Damiani et al.*, 2008, 2010; *Jackman et al.*, 2011; *Verronen et al.*, 2011]. The enhanced production of HO_x species is due to water cluster ion chemistry, a result of particle impact ionization, which leads to dissociation of water molecules. This process is only effective below about 80 km, where enough water vapor is available [*Solomon et al.*, 1981]. There are several types of precipitating energetic particles, which are characterized by their source and energy. Of these, solar energetic protons and electrons from the outer radiation belt have such energies that they affect the mesosphere directly, while galactic cosmic radiation (GCR) and auroral electrons deposit most of their energy in the lower stratosphere and lower thermosphere, respectively. Solar proton events (SPE) originate from explosions that occur sporadically on the surface of the Sun [*Meyer et al.*, 1956]. During SPEs, high-energy protons are guided by the Earth's magnetic field into polar regions and the atmospheric responses are typically constrained to magnetic latitudes higher than 60° [e.g., *Rodger et al.*, 2006; *Verronen et al.*, 2007]. In contrast, energetic electrons do not reach the atmosphere directly from the Sun but are first stored inside the magnetosphere, e.g. in the radiation belts, and can be lost to the atmosphere through precipitation. Energetic electrons in the radiation belts span a very large energy range, with large fluxes at "medium" energies of about 100 keV, and often include relativistic electrons with energies >0.5 MeV. Extreme examples of relativistic electron energies would be 10 MeV or even beyond [*Gussenhoven et al.*, 1996], albeit with very small fluxes. Those electrons in the outer radiation belt can precipitate into the atmosphere at magnetic latitudes of about 55–72°, with precipitation becoming more significant during and following magnetic storms, which also accelerate particles in the radiation belts. The atmospheric penetration depth depends on the energy of the particle, e.g. protons/electrons with 4 MeV/100 keV and 40 MeV/3 MeV energy can reach 80 km and 50 km, respectively [see, e.g., *Turunen et al.*, 2009, Figure 3]. Compared to the SPE phenomenon, our understanding of the importance of energetic electron precipitation to atmospheric chemistry is limited. This is mostly because accurate assessments of electron fluxes and temporal variability are difficult to make due to the spatial and temporal limitations of the observations and, sometimes, contamination of electron data by low-energy protons [*Rodger et al.*, 2010a; *Clilverd et al.*, 2010]. For example, the direct effects of electron precipitation in the mesosphere are not well quantified. Case studies have shown mesospheric odd nitrogen (NO_x) increases related to electron precipitation at high latitudes, but the relatively long chemical lifetime (∼months) of NO_x in polar winter conditions complicates the separation between in-situ production and atmospheric transport [*Sinnhuber et al.*, 2011].

[4] Recently, *Verronen et al.* [2011] have provided evidence of the connection between precipitating radiation belt electrons and mesospheric hydroxyl. They demonstrated strong correlation between experimentally observed 100–300 keV electron count rates (ECR) and nighttime OH concentrations at 70–78 km for two time periods, March 2005 and April 2006, at geomagnetic latitudes of 55–65°. In this paper, we extend their analysis and cover the time period between August 2004 and December 2009 (65 months) for which OH data from MLS are available. We go on to utilize the Sodankylä Ion and Neutral Chemistry (SIC) model and partial correlation analysis in order to separate the electron effect in OH from seasonal changes in water vapor, solar radiation, and temperature.

2. Data Description

[5] In addition to OH and precipitating electron data, we also use H_2O, temperature, and solar Lyman-α observations in our analysis. OH production in the middle mesosphere is mostly due to H_2O photodissociation by Lyman-α radiation. Although under nighttime conditions HO_x production is very limited, the HO_x produced during daytime can last some time after sunset depending on its chemical lifetime. Therefore, it is necessary to understand changes in the daytime production that could affect our nighttime analysis. Also, changes in temperature may lead to significant changes in OH through changing the rates of chemical reactions. More details and some characteristics of the MLS, solar Lyman-α, and electron data sets we make use of are given below and in Table 1.

[6] We excluded X-ray radiation from our analysis after checking the 0.1–0.8 nm data from GOES satellites. If any X-, M-, or C-class flares occurred during the analyzed time period, they could significantly increase the ionization in the mesosphere and affect OH mixing ratios. However, no X-class flares took place, the three periods of M-class flares were already excluded because of SPEs (see section 2.3), and there were no ECR data available for the C-class flare periods. Therefore, we can assume that X-rays do not interfere with our analysis.

2.1. MLS Observations

[7] In this study, we utilize observations from the MLS instrument onboard the Aura satellite [*Waters et al.*, 2006].

Table 2. Pressure Levels of the MLS Observations and Corresponding Approximative Altitudes

Pressure (hPa)	Altitude (km)
4.642	38
3.162	40
2.154	43
1.468	46
1.000	49
0.681	52
0.464	55
0.316	58
0.215	60
0.147	63
0.100	65
0.068	68
0.046	70
0.032	73
0.022	75
0.015	78
0.010	80
0.007	82
0.005	84

We use Version 3.3 Level 2 nighttime (solar zenith angle > 100°) OH, H_2O, and temperature data for the time period of August 2004–December 2009, concentrating on geomagnetic latitudes 55–65° in both the Northern and Southern hemispheres. Before the analysis, the data were screened according to the MLS data description and quality document [*Livesey et al.*, 2011]. More information on these MLS data products is given elsewhere [*Livesey et al.*, 2011; *Pickett et al.*, 2008; *Schwartz et al.*, 2008; *Lambert et al.*, 2007]. Most of the analysis has been made at the altitude range between 70–78 km. Note that in this study we discuss the MLS observations using an altitude (km) grid. The altitudes given are approximative and correspond to the pressure levels of the MLS observations, as shown in Table 2.

2.2. Solar Lyman-α

[8] Daily fluxes of composite solar Lyman-α radiation are available from Lasp Interactive Solar Irradiance Data Center (http://lasp.colorado.edu/lisird/lya/, accessed in April 2011). Time series for 2004–2009 were formed using solar irradiance measurements provided by the Solar EUV Experiment (SEE) instrument onboard the NASA Thermosphere Ionosphere Mesosphere Energetics and Dynamics (TIMED) spacecraft and the Solar Stellar Irradiance Comparison Experiment (SOLSTICE) launched as part of the Solar Radiation and Climate Experiment (SORCE). The amount of radiation at a certain latitude and altitude varies with the solar zenith angle (SZA), and we included this SZA dependency in the Lyman-α radiation using an exponential function of the secant of the SZA, i.e.,

$$I_{\alpha}^{SZA} = I_{\alpha} \exp[-\beta \sec(\phi)], \quad (3)$$

where $\sec(\phi) = 1/\cos(\phi)$, ϕ is the minimum SZA (maximum intensity of solar UV radiation) at 75 km for the corresponding day and location, and β is a fit parameter related to the optical depth for photodissociation [see *Minschwaner et al.*, 2011]. In our analysis we are interested only in the change of solar radiation and assume $\beta = 1$.

2.3. Energetic Particles

[9] We consider the ECR from the MEPED instrument onboard the Polar Orbiting Environmental Satellite (POES). For more information on MEPED, see *Evans and Greer* [2004]. We utilize data from the 0° detector pointing radially outwards along the Earth-satellite direction at L shells 3.0–5.5, which correspond to the geomagnetic latitudes of 55–65° and the locations of the inner and mid parts of the outer radiation belt. For magnetic latitudes above about 33°, the MEPED 0° directed telescopes are observing inside part of the bounce loss cone [*Rodger et al.*, 2010a, 2010b], and therefore monitoring a proportion of the particles precipitating into the atmosphere.

[10] The ECR measurements are considered the same way as in *Verronen et al.* [2011], except that a new correction algorithm for low-energy proton contamination has been applied (as described in *Lam et al.* [2010]) to decrease the significance of the contamination in the energetic electron measurements [*Rodger et al.*, 2010a]. As in *Verronen et al.* [2011], the count rates of the >300 keV energy channel are subtracted from those of the >100 keV channel to get an estimate of the flux of precipitating 100 to 300 keV electrons which will deposit the majority of their energy into the atmosphere at altitudes of 70–80 km. Note that these energy channels of the MEPED electron data are correlated with each other. Also, a similar response can be seen in the MEPED observations concerning relativistic electrons (E > 0.5 MeV) [*Rodger et al.*, 2010a; *Millan et al.*, 2010], which would increase ionization rates below 70 km. Because of this relation, we investigate also the lower mesospheric and stratospheric altitudes using the 100–300 keV count rates. We then support this approach by additional analysis of relativistic electron impacts using the MEPED P6 proton detectors.

[11] The MEPED P6 proton detectors respond also to highly relativistic electrons [*Rodger et al.*, 2010a]. However, the usability of the data is limited because of severe instrumental issues. The MEPED P6 omnidirectional detector responds to electrons with energies larger than about 800 keV but it has a varying detection efficiency with energy. It also responds to both trapped as well as drift- and bounce loss cone particles and is therefore not well suited for understanding electron precipitation. Like the omnidirectional one, also the P6 0° detector responds to energies with a varying detection efficiency, starting from electrons with energies roughly larger than about 700 keV. In addition, the P6 0° detector often report fluxes near the noise floor of the instrument, and only report substantial relativistic electron precipitation fluxes during stronger events. Because of these issues, we use the P6 data only to support the analysis based on the 100–300 keV data.

[12] Monthly and daily mean count rates are calculated from the data, which originally was produced with a 3-hour temporal resolution from the 2 s resolution files available from NOAA. We assume that electron forcing is more or less the same for both hemispheres, particularly during geomagnetic storms which have high electron precipitation fluxes, and thus the mean MEPED-reported precipitating fluxes are determined from all available POES spacecraft located inside the L-shell range 3–5.5 in either hemispheres. The same assumption was made by *Verronen et al.* [2011].

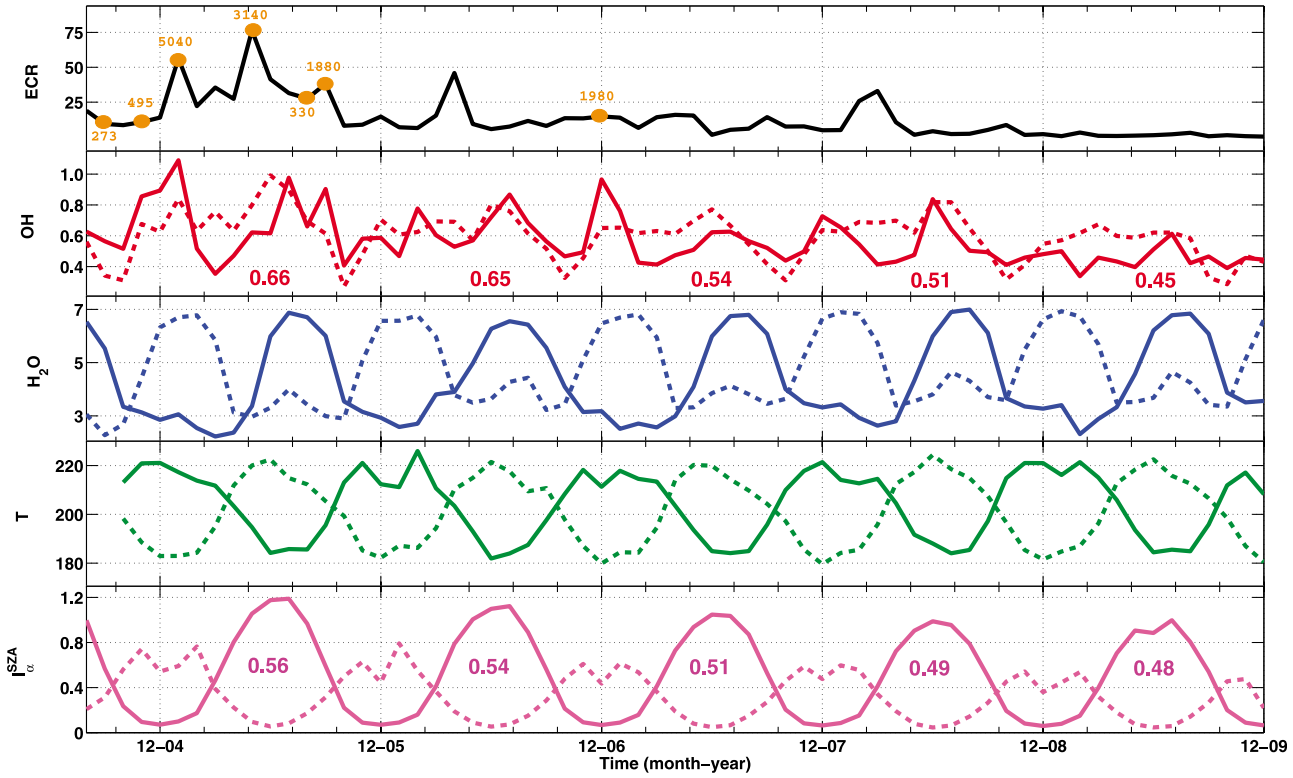

Figure 1. (top to bottom) Monthly mean ECR (counts/s), nighttime OH (ppbv), H_2O (ppmv), temperature (K), and I_α^{SZA} (10^{11} photons/cm^2/s). OH, H_2O, and temperature are averages between geomagnetic latitudes 55–65°N (solid lines) and 55–65°S (dashed lines) at altitude 75 km (0.022 hPa). All panels show the time period August 2004–December 2009. Solar proton events are indicated in the top panel by orange circles with the corresponding numbers representing the magnitude in particle/cm^2/s/sr units. Red/violet numbers indicate yearly mean OH/I_α^{SZA} from 2005–2009 in the NH.

We do, however, exclude from the mean any measurements taken from POES spacecraft located inside the South Atlantic Magnetic Anomaly, due to contamination concerns. In addition, electron fluxes measured during SPEs are excluded from our analysis, because the electron observations are not reliable at these times. We use two data sets to identify and exclude the SPE time periods: (1) the list of solar proton events and their magnitudes from NOAA Space Environment Services Center (http://www.swpc.noaa.gov/ftpdir/indices/SPE.txt, accessed in March 2011), and (2) the >5 and >10 MeV proton fluxes from Geostationary Operational Environmental Satellite (GOES-11).

3. Results

[13] Zonal monthly mean values of OH, H_2O, temperature (T) together with I_α^{SZA}, ECR, and solar proton events presented in Figure 1 give a general view on the OH variation at 75 km altitude. The OH mixing ratio shows a much more complex temporal behavior than H_2O, I_α^{SZA}, and T, and its variability cannot be explained by seasonal effects only. Time series of H_2O, temperature and I_α^{SZA} display a clear annual periodicity. H_2O amounts are higher in the summer because the pole-to-pole mean circulation, i.e., upwelling, transports H_2O-rich air from below. In the winter, transport is from above (downwelling) and leads to lower H_2O amounts. Temperature behavior is the opposite, because adiabatic heating/cooling takes place during downwelling/upwelling periods. The I_α^{SZA} asymmetry between the Northern hemisphere (NH) and Southern hemisphere (SH) is a direct consequence of geomagnetic latitude selection which corresponds to a different set of solar zenith angles in the two hemispheres. Although I_α^{SZA} shows the transition from high to low solar activity between 2004–2009, the SZA-modulation leads to much stronger seasonal variation similar to that of H_2O, with high I_α^{SZA} values during summer. In contrast, the OH time series exhibits spikes, which seem to coincide with particle forcing especially during the SPE periods. The general decrease of OH with time shows that the changes in OH are consistent with declining solar activity [see also *Shapiro et al.*, 2011]. The mean value of the OH mixing ratio during the period August 2004 to May 2007 is about 23% larger in the NH and about 10% larger in the SH than June 2007 to December 2009. The OH and I_α^{SZA} variations in the NH (solid lines) are supported by yearly means of OH and I_α^{SZA} from 2005–2009 (red and violet numbers) which show a decreasing trend through all the years. Similar effects can be observed in the SH, however they are less pronounced than in the NH. Note that the monthly mean ECR shows a decreasing trend of the electron fluxes in the radiation belts [see also *Farr et al.*, 2009].

[14] Compared to the SPEs effects, which are strong and easier to detect, the OH increases during peaks of electron precipitation are smaller in magnitude and thus more

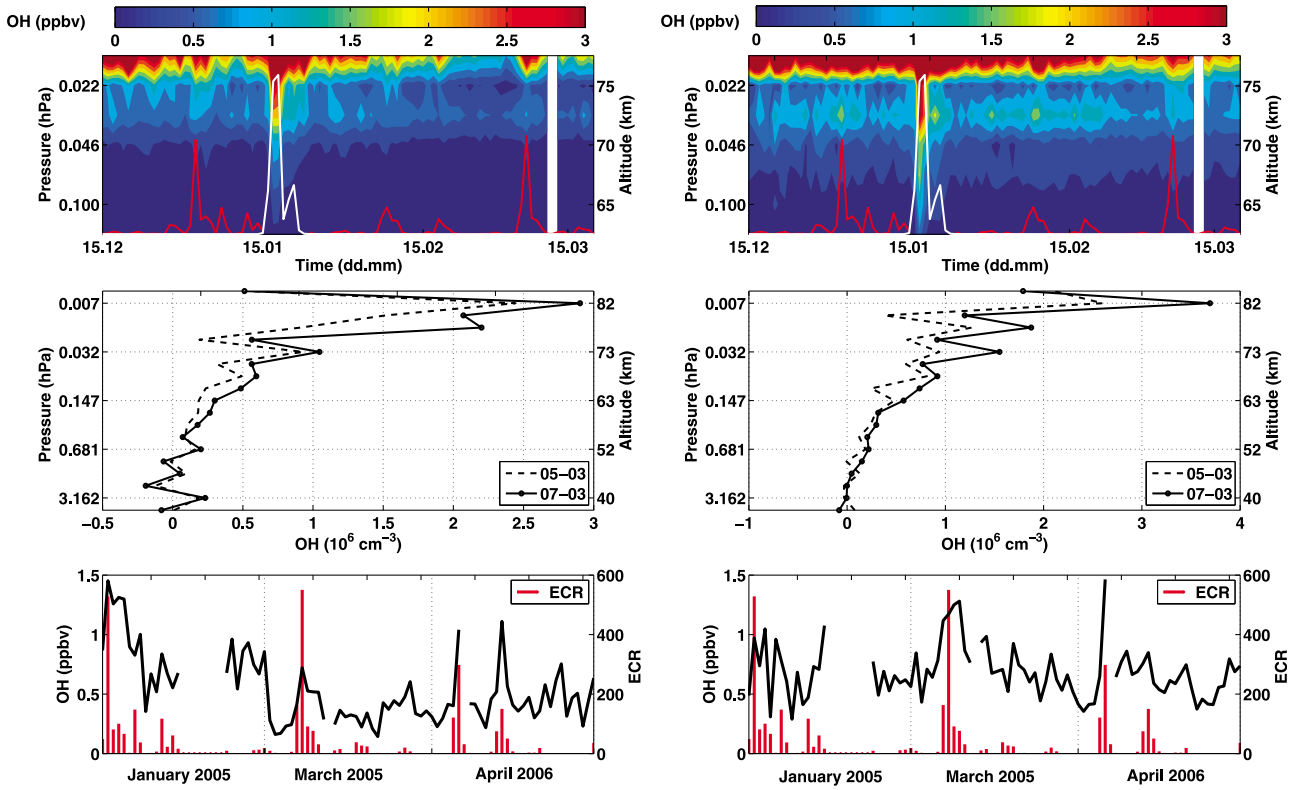

Figure 2. (top) Daily mean OH mixing ratio (ppbv) at geomagnetic latitudes 55–65° shown for altitudes 63–78 km (0.147–0.015 hPa) for the period 15th of December 2004 to 15th of March 2005. Daily mean ECR is marked with a red line and daily mean proton fluxes are marked as white line. (middle) OH concentration (10^6 cm^{-3}) during EEP event on March 7 2005 (solid line), and OH concentration (10^6 cm^{-3}) before EEP event on March 5 2005 (dashed line) shown for altitudes 38–85 km (0.681–0.005 hPa). (bottom) Daily mean OH mixing ratio (ppbv) shown for altitude 75 km (0.022 hPa) for January 2005, March 2005 and April 2006. Daily mean ECR is marked as a red stem. (left) NH and (right) SH.

difficult to identify using monthly mean data, where the seasonal variation of H_2O and I_α^{SZA} dominates, and confident conclusions cannot be made. Removing SPE periods from the data sets does not significantly help our analysis (not shown). The short chemical lifetime of OH and substantial day-to-day variations in ECR are likely the reason that ECR has no detectable impact on OH monthly averages. Therefore, in the following we continue our investigation using daily mean data instead of monthly means. Again, all the MLS daily averages were calculated using nighttime measurements only.

[15] In Figure 2 we show the daily mean OH mixing ratio for the NH and the SH from 15th of December 2004 to 15th of March 2005 together with the daily mean ECR and daily mean proton fluxes. We can clearly see the OH increases in both hemispheres at altitudes above 70 km during the peak of the ECR in January 2005 and March 2005 (2nd of January and 7th of March, respectively). Note that the observed OH response to the precipitating electrons is weaker in comparison to the SPEs observed in the middle of January (17th of January). Figure 2 (middle) presents two OH vertical profiles between 38–85 km from March 2005: (1) 5th of March (low ECR, low OH concentration) and (2) 7th of March (high ECR, high OH concentration). When high ECR are observed the OH concentration clearly increases above 63 km in both hemispheres. The OH increase of up to 100% is highest for the altitude range between 75–78 km in the NH and for 75–82 km in the SH. The bottom panel of Figure 2 shows the time series of daily mean ECR together with daily mean OH mixing ratio at 75 km altitude for January 2005, March 2005 and April 2006. It is clear that OH responds to increases in ECR without any significant time delay.

[16] We calculated Pearson's product–moment correlation coefficients using daily mean data of ECR and OH. We did the calculations separately for each month and each of the 19 pressure levels of MLS observations between 38–85 km. In the correlation analysis we do not consider data uncertainties, because in the high-correlation cases they are typically small compared to the variations in ECR and OH. The Pearson's correlation method assumes a linear relationship between the variables. Although OH mixing ratio is not expected to increase exactly linearly with electron flux [e.g., *Verronen et al.*, 2011], it should increase monotonically so that the Pearson's method can be used in our analysis. To test this we repeated the correlation coefficient calculations using a $\sqrt{\mathrm{ECR}}$ dependence (which was used by *Verronen et al.* [2011]). The calculated correlation coefficients were very similar to those assuming a linear relationship, with maximum of 5–10% differences in few cases only. Because of this, and because the full functional dependence between

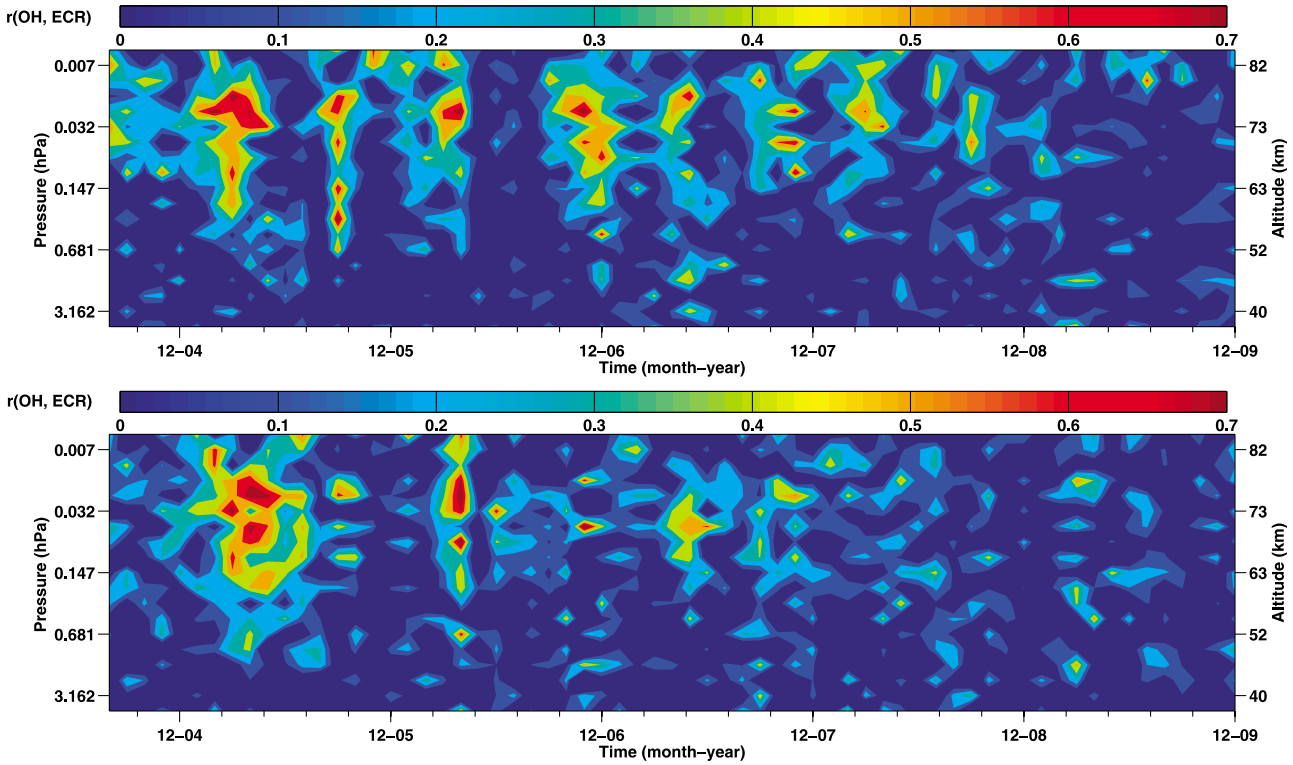

Figure 3. Correlation coefficient r between daily mean OH mixing ratio and daily mean ECR. Altitudes 38–85 km (4.642–0.005 hPa) are shown between August 2004–December 2009 at geomagnetic latitudes (top) 55–65°N and (bottom) 55–65°S.

OH mixing ratio and ECR is not easily solved, we retained the direct Pearson's correlation calculation as an appropriate and practical approach. As a first check, the statistical robustness of the correlation was determined by calculating the p value (t-test), i.e., the random chance probability of getting such correlation for the data sets when the true correlation is zero. 95% confidence level, i.e., $p \leq 0.05$, corresponds to correlation coefficient values equal or larger than 0.35. Correlation values above 0.52 with $p < 0.01$ we consider as highly correlated.

[17] Figure 3 shows the correlation between daily mean OH mixing ratio and daily mean ECR precipitating from the radiation belts. Note that the SPE periods were excluded here and from all further considerations using a flux limit of 4 protons/cm^2/s/sr (GOES-11, 5–10 MeV channel). The results shown in Figure 3 clearly demonstrate that correlations between OH and precipitating electrons is high for almost all the months with days of very high ECR. However, there are differences in temporal and altitude responses between the NH and the SH.

[18] At 75 km in the NH, for 22 months (34%) of the total of 65 analyzed, the correlation r is equal or higher than 0.35, and in 10 of those cases $r \geq 0.6$. The characteristics of the eleven highest-correlation cases are listed in Table 3. Almost all months with the maximum of daily mean ECR $\geq$ 150 have $r \geq 0.6$. However, the correlation does not always increase linearly with the amount of electrons precipitating into the atmosphere, because it is also affected by background atmospheric conditions, i.e., the amount of background OH and, to a lesser extent, day-to-day changes in H_2O, I_α^{SZA}, and T. Very high correlation coefficients (higher than 0.77) are sometimes reached between 70–78 km, e.g. in February 2005, April 2006, and November 2006. In addition to the small changes in H_2O, I_α^{SZA}, and T which can influence the correlation calculation, all cases with $r > 0.71$ have favorable conditions for ECR detection, i.e.,: (1) either very high ECR (>300 count/s) or modest OH background mixing ratios, and (2) low median of ECR daily means. Note that during 2009 when solar activity and ECR were exceptionally low, also the correlation is generally low. The negative correlation in November 2006 in the SH is related to the single day with negative OH at 75 km coinciding with high ECR.

[19] In general, Figure 3 shows correlations $r \geq 0.35$ down to 52 km during months of high ECR. Above 78 km correlation decreases due to smaller amounts of water vapor (and water cluster ions/HO_x produced during EEP), and also because the nighttime OH maximum at about 82 km makes EEP effects more difficult to detect [see also *Verronen et al.*, 2011]. Below 52 km, for most cases, r does not exceed 0.2, which suggests that the fluxes of >3 MeV electrons are not sufficiently high to increase the OH mixing ratios at these altitudes, at least within the experimental uncertainties of these measurements. Because this result is based on the 100–300 keV electron data (electrons with these energies affect mainly the altitudes between 70–80 km), we calculated also correlations r^P between OH and count rates from MEPED P6 detectors (both omnidirectional and 0°). These detectors respond to highly relativistic electrons (with energies larger than about 700 MeV), but there are instrumental issues that limit their usability (see section 2.3). Nevertheless, we found that at altitudes below 52 km r^P is generally very small, i.e.,

Table 3. Characteristics of the Months Showing Highest OH-ECR Correlation at 75 km and Geomagnetic Latitudes 55–65°N/S, With $r \geq 0.6$ in the NH and/or the SH[a]

Case	Time (mm-yy)	ECR^m	ECR^d (counts/s)	ECR^{med}	Gaps	OH^{med} (ppbv)	r	$R_{H_2O \cdot I_\alpha^{SZA},T}$	r^b	SE^b
1	01-05	57	528	17	8	0.90	0.60	0.46	0.57	0.14
						0.69	0.34	0.37	0.34	0.18
2	02-05	22	151	2	-	0.43	0.80	0.77	0.77	0.09
						0.63	0.37	0.47	0.35	0.23
3	03-05	36	550	3	-	0.33	0.60	0.71	0.57	0.15
						0.71	0.54	0.50	0.63	0.10
4	04-05	27	298	2	-	0.42	0.71	0.77	0.68	0.20
						0.64	0.76	0.76	0.67	0.21
5	05-05	77	789	9	4	0.52	0.25	0.32	0.30	0.13
						0.74	0.73	0.80	0.66	0.25
6	09-05	38	200	7	9	0.57	0.64	0.47	0.60	0.24
						0.49	0.64	0.43	0.66	0.10
7	03-06	15	176	1	-	0.60	0.62	0.68	0.63	0.09
						0.69	0.38	0.42	0.40	0.16
8	04-06	46	761	2	-	0.49	0.78	0.80	0.79	0.13
						0.67	0.80	0.84	0.67	0.29
9	11-06	13	208	1	-	0.44	0.79	0.80	0.73	0.16
						0.46	−0.42	−0.43	−0.32	0.25
10	11-07	8	150	0.7	-	0.46	0.72	0.72	0.58	0.31
						0.45	0.61	0.57	0.59	0.18
11	03-08	33	347	9	-	0.41	0.61	0.61	0.58	0.17
						0.68	0.18	0.58	0.20	0.11

[a]From left to right the columns are: case number, time (month-year), monthly mean ECR of the MEPED 100–300 keV energy channel, maximum daily mean ECR of the 100–300 keV energy channel, median of daily means of ECR, number of days with no data, median of daily means of OH, correlation coefficient r, partial correlation coefficient $R_{H_2O \cdot I_\alpha^{SZA},T}$, mean correlation of the bootstrap distribution r^b and bootstrap standard error SE^b. For each month, some parameters are given for both the NH (upper line) and the SH (lower line).

similar to the correlation between OH and ECR at 100–300 keV. This, again, indicates no significant electron impact on OH in the stratosphere.

[20] Compared to the NH, the SH response is in general less pronounced. r exceeds 0.6 only in 5 cases and is for some months significantly lower than in the NH (Table 3). Nevertheless, the number of months with $r \geq 0.35$ is similar to the NH, i.e. 20 of 65 months (31%, c.f., 34% in the NH). May 2005 is the sole case in Table 3 for which the correlation is significantly lower in the NH than in the SH, i.e. at 75 km $r = 0.25/p = 0.24$ and $r = 0.73/p \approx 0$, respectively. However, in this case high correlation is observed in the NH at a slightly lower altitude of 73 km ($r = 0.65$, Figure 3).

[21] To gain additional confidence in the calculated correlations, we tested the robustness of the results using the bias-corrected and accelerated bootstrap method. For each hemisphere-month-altitude combination, the correlation coefficient was calculated 200 times for a random distribution of all available data points. Then the bootstrap standard error SE^b and the mean correlation of the bootstrap distribution r^b were calculated. For most of the cases the bootstrap method indicates that the calculated Pearson's correlations are robust. For example, SE^b is generally smaller than 0.25, in 10% of the cases $SE^b > 0.25$ (mainly for months with lower ECR), and only about 4% exhibit $SE^b > 0.3$. Also, the difference between the Pearson's correlation r and r^b is on average less than 0.03. The details of bootstrap analysis for the 11 cases with the highest correlation coefficients are presented in Table 3. The bootstrap results are in good agreement with the Pearson's correlation calculations, except for November 2007 (NH) and April 2006 (SH) when the difference between r^b and r is larger (0.14 and 0.13, respectively) and $SE^b > 0.25$. In these two cases the Pearson's correlation seems to be less robust. Finally, 95% confidence intervals CI^b of r^b were calculated (not shown). All cases with a high Pearson's correlation and $p < 0.05$ (t-test) have a positive minimum of CI^b, which is strong quantitative evidence that the calculated correlations between OH and ECR are not coincidental.

[22] Figure 4 shows a comparison of OH mixing ratios for the NH and the SH in March 2008. This month was chosen for a closer inspection because it has the largest correlation discrepancy between the two hemispheres. Figure 4 (top) shows daily mean values of OH mixing ratios, and Figure 4 (bottom) shows three OH altitude profiles: (1) monthly mean, (2) day 27 mean (high ECR, high OH), (3) day 25 mean (low ECR, low OH). In both hemispheres, OH increases due to strong electron forcing (top panels), but the larger OH background mixing ratio in the SH makes the EEP-related changes more difficult to detect and leads to lower correlation coefficients. Figure 4 (bottom) shows that when high ECR are observed on day 27, the OH mixing ratios increase by about 50% between 70–78 km in both hemispheres compared to the day 25 with low ECR. However, the monthly mean OH value in the SH is higher than in the NH and close to the OH mixing ratio observed on day 27. Thus the EEP-related OH production is clearly more pronounced in the NH and the correlation is understandably higher. The hemispheric discrepancy in background OH level can be explained mainly by differences in water vapor and Lyman-α radiation as well as SZA which affects the number of profiles selected for daily averages. In addition, the temperature might also contribute to the NH-SH OH abundance asymmetry, however the effect of temperature on OH is not as straight forward to assess because temperature changes do not affect OH or HO_x reactions alone but the whole chemical system.

[23] In addition to affecting the correlation calculation through monthly mean background OH mixing ratios, OH changes due to intramonth variation of H_2O, I_α^{SZA}, and

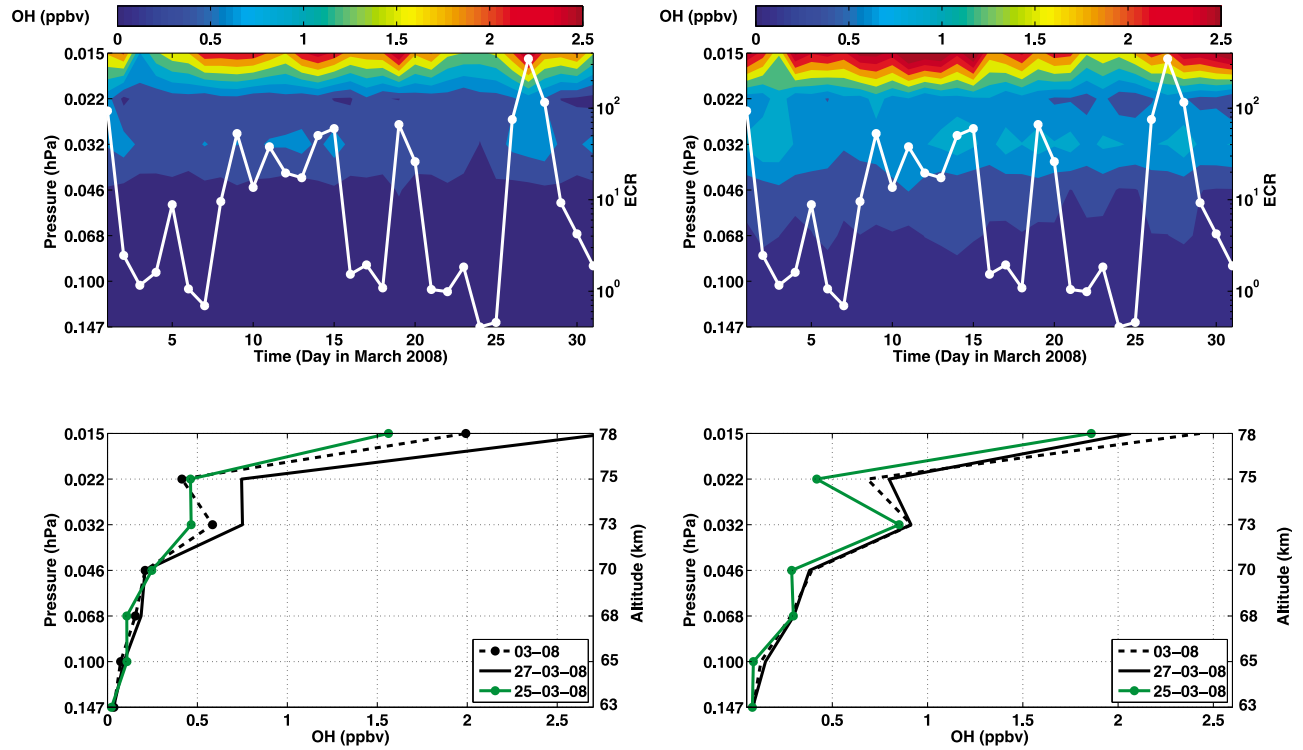

Figure 4. (top) Daily mean OH mixing ratio (ppbv) at geomagnetic latitudes 55–65° shown for altitudes 63–78 km (0.147–0.015 hPa) in March 2008. Daily mean ECR is marked with a white line. (bottom) Vertical profiles of OH mixing ratio (ppbv) for March 2008: monthly mean (dotted line), daily mean for day 27 during strong electron forcing (solid line), daily mean for day 25 during weak electron forcing (green line). (left) NH and (right) SH.

T could also mask the EEP effects. For this reason, we verified the robustness of our results using partial correlation analysis. The 1st-order partial correlations $R_{H_2O} = R(OH, ECR. H_2O)$ and $R_T = R(OH, ECR. T)$ which measure the correlation between daily OH mixing ratios and daily ECR, with the effect of H_2O and temperature removed, were computed from the regular correlation coefficient r (0th-order partial correlation), i.e.,

$$R_X = \frac{r(OH,ECR) - r(OH,X)r(ECR,X)}{\sqrt{1 - r(OH,X)^2}\sqrt{1 - r(ECR,X)^2}}, \quad (4)$$

where $X = H_2O$ or T. Similarly, 2nd-order partial correlation $R_{H_2O \cdot I_\alpha^{SZA},T} = R(OH, ECR. H_2O \cdot I_\alpha^{SZA}, T)$ was calculated with the product of I_α^{SZA} and H_2O as well as T taken as controlled variables. The differences between partial and ordinary correlations are shown in Figure 5 and Table 3.

[24] Figure 5 presents the differences $R_{H_2O} - r$ (Figure 5, top) and $R_T - r$ (Figure 5, bottom) for both the NH and the SH. Between 65–75 km the differences are in general small, i.e., on average absolute differences are smaller than 0.04/0.05 in the NH/SH. Also, the calculated absolute difference $R_{H_2O \cdot I_\alpha^{SZA},T} - r$ (shown in Table 3) is on average less than 0.06/0.07 in the NH/SH. This is again a small difference, but it should be noted that for most of the 11 cases presented in Table 3, $R_{H_2O \cdot I_\alpha^{SZA}}$ is higher than r and indicates less difference between the hemispheres. Overall, the ordinary correlation is a sufficient tool for our analysis, and we can in most cases assume that $r \cong R$. However, in some months, such as March 2005, September 2005 and March 2008, large differences exist especially in the SH. These seem to take place mostly during spring and autumn periods, when the strongest seasonal changes in H_2O, I_α^{SZA}, and T occur.

[25] Taking March 2008 as an example, no differences were observed between partial correlation R_{H_2O} and ordinary correlation r in the NH (Figure 5, top left). In the SH, the difference $R_{H_2O} - r$ is positive, which means that relationship between ECR and OH is stronger when the effect of H_2O changes is considered. In case of temperature, there is again no significant difference between partial correlation and ordinary correlation in the NH. In the SH, the difference $R_T - r$ is positive and high, and suggests an increase of the correlation between ECR and OH when temperature is fixed. Similar effects are observed when controlling H_2O and temperature together with I_α^{SZA} (partial correlation $R_{H_2O \cdot I_\alpha^{SZA},T}$ in Table 3). In other months, water vapor and temperature changes can also enhance the OH-EEP correlation. For example, in September 2005 the difference $R_T - r$ in the SH is negative and high (Figure 5, bottom right) which indicates that a part of the correlation r calculated between electrons and OH was actually caused by temperature changes. Overall, based on Figure 5, the effect of H_2O and temperature on the OH-EEP correlation is stronger in the SH, and temperature seems to have a stronger effect than H_2O.

[26] In order to verify the sensitivity of OH to H_2O and temperature in March 2008 we used the Sodankylä Ion and

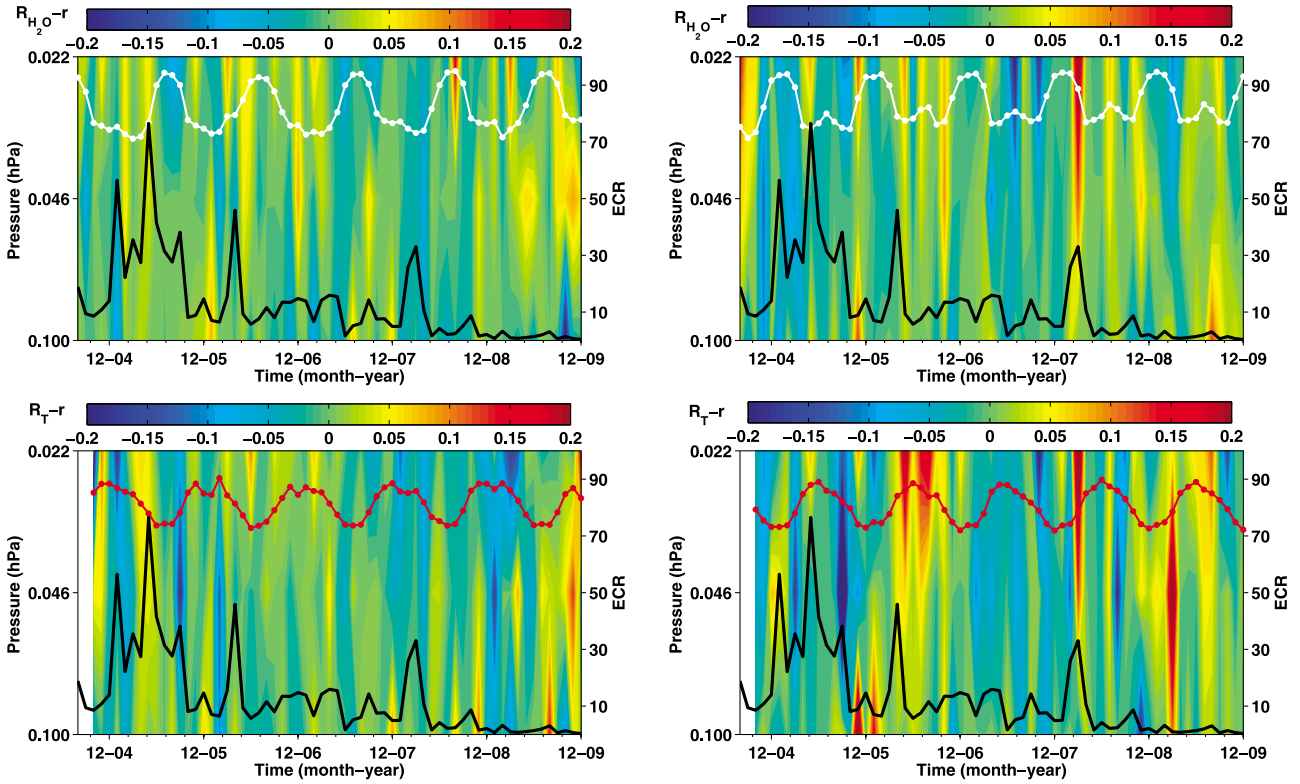

Figure 5. (top) Difference between partial correlation coefficients R_{H_2O} and correlation coefficients r at geomagnetic latitudes 55–65° shown for altitudes 65–75 km (0.1–0.022 hPa). Panels include daily mean ECR (black lines), monthly mean water vapor (white lines) and temperature (red lines). (bottom) Same as Figure 5 (top) with R_T instead of R_{H_2O}. (left) NH and (right) SH.

Neutral Chemistry model (SIC). SIC is a 1-D model of the middle atmosphere and includes a complete set of HO_x chemistry. Transport processes are not considered in the model, except for vertical diffusion. However, because the chemical lifetime of HO_x at 75–80 km altitudes is between 0.1–1 day [*Pickett et al.*, 2006], atmospheric transport of HO_x below 80 km is negligible and SIC is a sufficient tool for this study. A detailed description of the model is given by *Verronen et al.* [2005] and *Verronen* [2006]. All model runs were made for the 15th of March 2008 at 60°N/S and 0°E. First, we made model runs using MLS monthly mean values of H_2O and temperature. Then we changed H_2O and temperature according to the variability observed by MLS in March 2008. Figure 6 (top) shows that by changing H_2O by 15% in the NH and by 50% in the SH, the nighttime OH mixing ratio changes by about 5% and 15%, respectively. The decrease of OH with decreasing amounts of H_2O is a direct consequence of decreasing photodissociation reaction rates. OH concentration is more sensitive to changes in temperature than those of H_2O (Figure 6, bottom). Temperature increases by 5% in the NH and changes nighttime OH mixing ratio in average by about 5% while in the SH the temperature increases by 15% and changes the nighttime OH mixing ratio in average by about 20%. The effect of temperature on OH is related to the changes in chemical reaction rates. For both H_2O and T, at nighttime the sensitivity is modest compared to daytime, which indicates a better possibility of identifying EEP effects at night.

[27] Summarizing the correlation analysis, Figure 7 (top) illustrates the correlation coefficients r and partial correlation $R_{H_2O \cdot I_\alpha^{SZA},T}$ (presented in Table 3) for 75 km sorted in ascending order by monthly mean ECR. It is evident that in general the correlation increases with increasing ECR. In the NH, in cases when monthly mean ECR is higher than about 8 counts/s, almost 60% of the correlation coefficients exceed 0.35 and thus have a random chance probability less than 5%. This proportion increases up to 77% for cases with ECR higher than 15 counts/s. In contrast, during months which have mean ECR less than 8 counts/s, the EEP does not seem to have significant influence on OH. The negative correlations among the high-electron-count periods are, in most of the cases, related to the strong H_2O and solar radiation variation, especially during the periods of H_2O increase between May–July.

[28] The results obtained for the SH show a similar behavior to the NH, i.e., the correlation generally increases with ECR. However, the overall correlation is slightly smaller, so that about 50%/71% of cases with monthly mean ECR higher than 8/15 count/s have r equal or larger than 0.35. In contrast, ECR-sorted time series of H_2O, I_α^{SZA} and temperature do not show any increasing trend with increasing ECR (not shown).

[29] Figure 7 (bottom) provides a similar analysis for the correlation between OH and the product of H_2O and I_α^{SZA}, $r(OH, H_2O \cdot I_\alpha^{SZA})$. In this case, the correlation dependency on the amount of electron precipitation is random, no clear

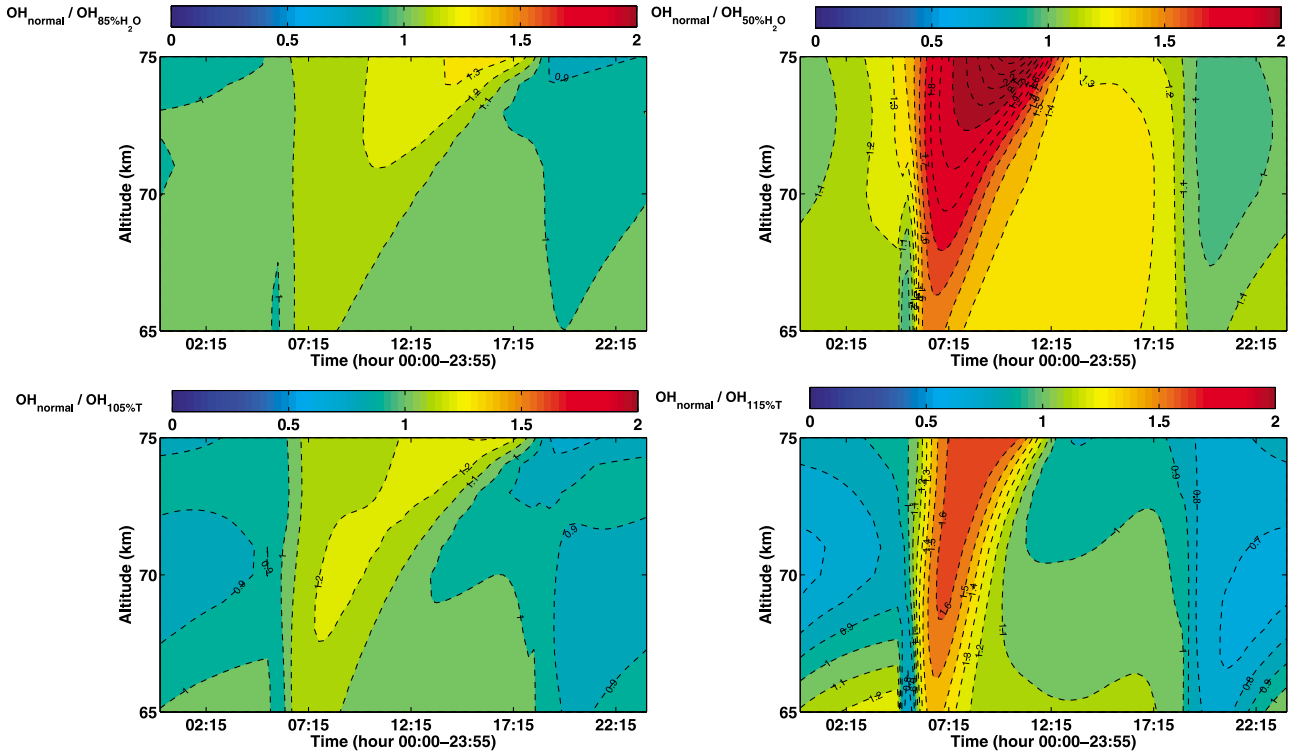

Figure 6. SIC model results for March 15, 2008 between 65–75 km (0.1–0.022 hPa). (top) OH ratio between a model run using MLS-observed water vapor and model runs with 85% (NH) and 50% (SH) of the observed H_2O. (bottom) OH ratio between a model run using MLS-observed temperature and model runs with 105% (NH) and 115% (SH) of the observed temperature. (left) NH and (right) SH.

patterns similar to those shown in Figure 7 (top) are present. Therefore, it is clear that the increasing trend in the correlation between OH and ECR does not coincide with the increasing trend in the correlation between OH and the product of H_2O and I_α^{SZA}. Thus, we can conclude that the electron precipitation is the most likely driver of the observed OH increases.

[30] In Figure 8 we show the monthly correlation coefficients r between OH and ECR, versus monthly mean ECR at 75, 65, and 47 km altitudes. Note that the 75-km data are the same as those shown in Figure 7 (top). Figure 8 also shows linear fits (least-squares method) made to the data, which clearly show an increase in r with increasing ECR for altitudes 65 and 75 km. We have calculated the correlation rr between correlation r and monthly mean ECR, giving us a quantitative measure of the connection between them. At 75 km, there is a clear dependency of r on monthly mean ECR with rr values 0.44/0.54 in the NH/SH. So, although r is in general higher in the NH, rr is higher in the SH. This indicates a stronger linear relation between correlation r and ECR in the SH, even though the OH enhancements due to electron impact are not as pronounced as in the NH. At 65 km, the increase in r with increasing ECR is still detectable, although not as pronounced as at 75 km. The rr values are lower, 0.18/0.40 in the NH/SH, and the random chance probability is significant in the NH. At 47 km (and at altitudes below), r does not show an increase with increasing monthly mean ECR, and rr is close to zero in both hemispheres, which again indicates a negligible effect on OH by >3 MeV electron precipitation.

[31] In order to assess the latitudinal extent of EEP-related OH enhancements, we also examined the correlation between OH and ECR at other geomagnetic latitude bands, exactly as we did for the band 55–65°. Daily mean OH was correlated with radiation belt daily mean ECR for the geomagnetic latitude ranges of 35–45°, 45–55°, and 65–72° (i.e., shells from L = 1.5 to L = 10). The POES satellites spend little time at the highest geomagnetic latitudes, and there are not enough ECR data available from latitudes >72° for a proper analysis. This restricts our study to lower geomagnetic latitudes. Figure 9 shows the results obtained for the 11 cases presented in Table 3, i.e., those with the highest OH-ECR correlation at 75 km altitude in the band 55–65°. In the NH, the strongest correlation is observed at 55–65° for all cases. Correlation for the band 65–72° is in many cases similar, although always lower. At the other latitude bands we consider here, the correlation is clearly lower. In the SH, the highest correlations are also found at 55–65°, but there are several cases where the correlation at 65–72° is slightly higher. For the lower geomagnetic latitudes, the correlation is in general low (below 0.35). Therefore, we can conclude that for the cases considered, EEP clearly affects magnetic latitudes 55–72°, and the lower latitudes are influenced much less. This kind of latitudinal response is within expectations, because the outer

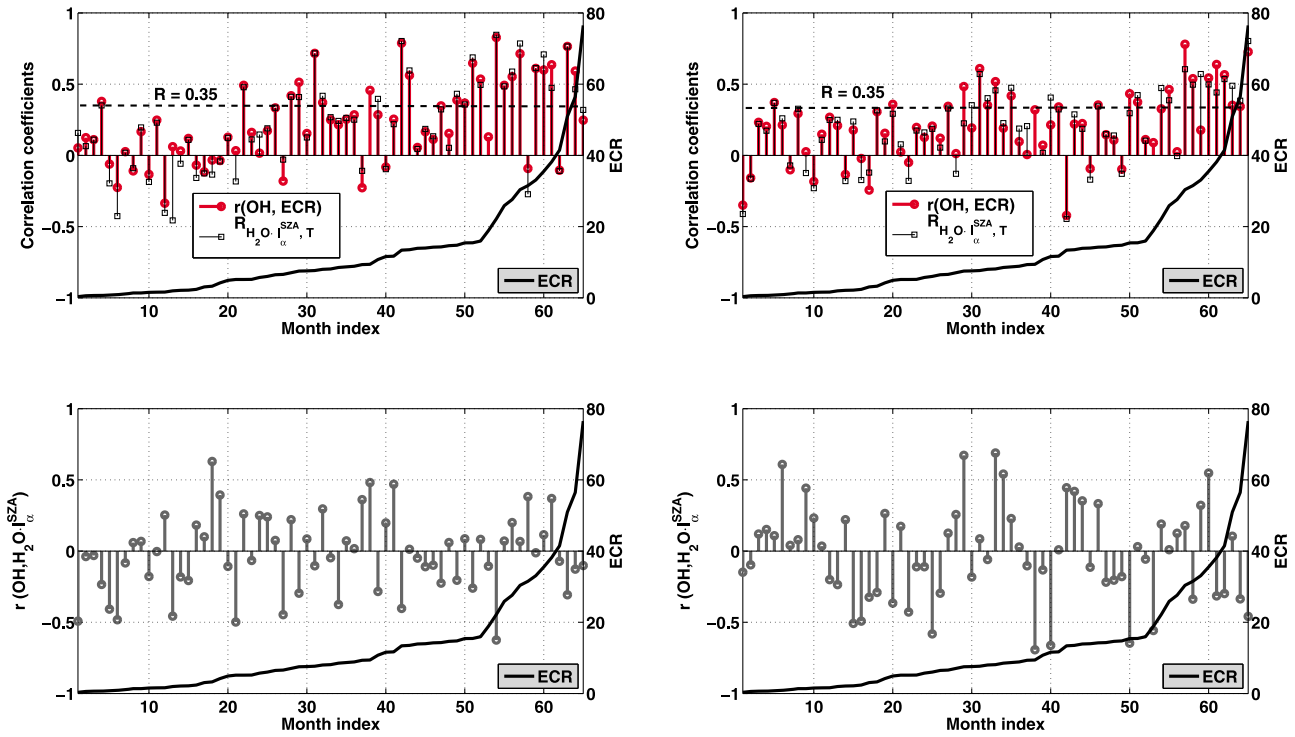

Figure 7. (top) Correlation r (red bar) and partial correlation $R_{H_2O \cdot I_\alpha^{SZA},T}$ (black bar) between OH and ECR at 55–65° shown for altitude 75 km (0.022 hPa) sorted in ascending order by monthly mean ECR. (bottom) Same as Figure 7 (top) but showing correlation $r(OH, H_2O \cdot I_\alpha^{SZA})$. (left) NH and (right) SH.

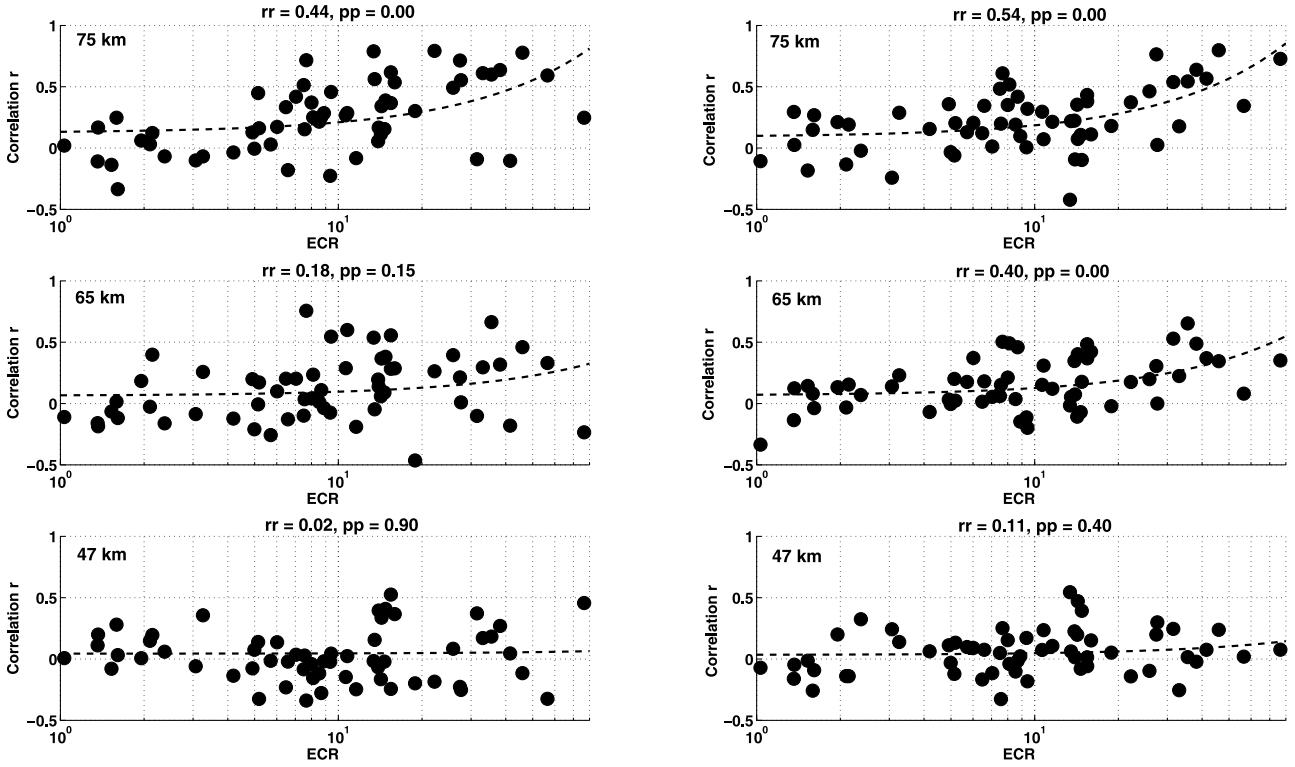

Figure 8. Correlation coefficients r(OH, ECR) versus monthly mean ECR at 55–65° shown for (top) 75 km, (middle) 65 km, and (bottom) 47 km. The dashed lines show a linear fit to the data at each altitude. In panel titles, *rr* = correlation coefficient between r and ECR, and *pp* = random chance probability of getting such correlation for the data sets when the true correlation is zero. (left) NH and (right) SH.

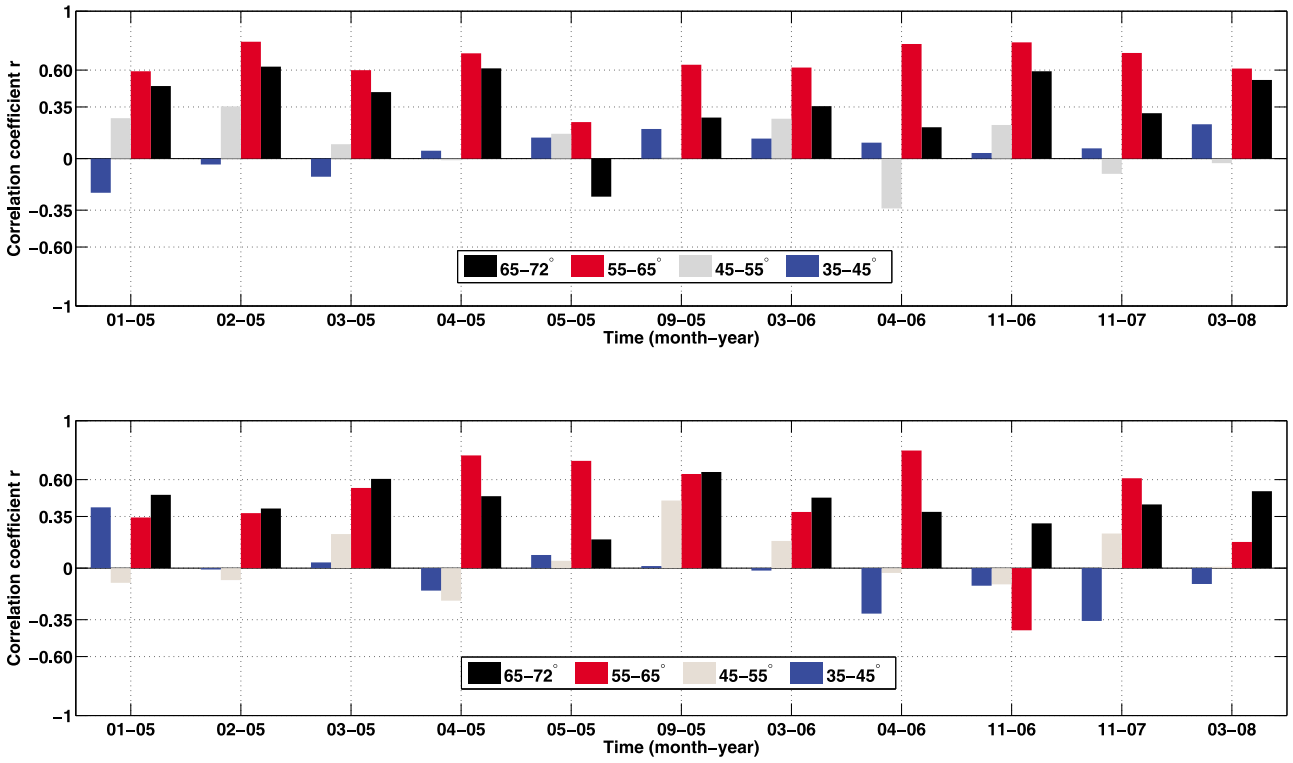

Figure 9. Correlation coefficient r between daily mean OH mixing ratio at 75 km (0.022 hPa) and daily mean ECR at 35–45°, 45–55°, 55–65° and 65–72° geomagnetic latitudes shown for all months presented in Table 3. (top) NH and (bottom) SH.

radiation belt is connected approximately to magnetic latitudes 55–72°.

4. Conclusions

[32] Analyzing daily time series of MLS OH mixing ratios and MEPED radiation belt electron precipitation rates during the period August 2004–December 2009 at 55–65° geomagnetic latitudes in both hemispheres, we have studied the connection between electron precipitation and middle atmospheric OH enhancement. Our correlation analysis shows that between 70–78 km altitudes in 22 out of 65 months (34%) in the NH and in 20 out of 65 months (31%) in the SH, the correlation is statistically robust ($r \geq 0.35$, $p \leq 0.05$) and indicates a measurable EEP effect on OH. In cases with monthly mean ECR higher than 8 counts/s, the fraction of months with clear EEP influence increases to about 55% in the NH and about 49% in the SH. At 75 km, 10/5 months in the NH/SH with maximum daily mean ECR exceeding or equal to 150, on at least one day, have correlation equal or higher than 0.6. Moreover, EEP effects are easiest to detect during the months with especially low OH background or high electron forcing, combined with low ECR median value. In these cases, correlation can exceed 0.77, indicating that more than 50% of OH variation can be explained by the electron precipitation.

[33] The correlation between OH and ECR is also generally weaker in the SH than in the NH. In most cases, the hemispheric differences are caused by higher OH background mixing ratios or stronger water vapor and temperature influence in the SH, which make EEP-related OH changes more difficult to be detected. In 50% of the cases that have large differences between the NH and the SH, accounting for the effects of H_2O, solar radiation, and temperature using partial correlation analysis improves the correlation and reduces hemispheric asymmetries.

[34] Correlation between ECR and OH is observed between 52–70 km, i.e., at altitudes that are affected by 100 keV–3 MeV electrons. At altitudes above 80 km the amounts of water vapor are too low for efficient cluster ion formation and ionic HO_x production and the observed correlation is not significant. Below 52 km there is no evident correlation between ECR and OH, which suggests that, at least in the 2004–2009 time period studied here, >3 MeV electrons do not have a detectable impact on OH in the stratosphere. In addition, correlation at lower geomagnetic latitudes bands, i.e., 35–45° and 45–55° are in general lower than 0.35, but higher than this for higher latitudes. Our study indicates that EEP primarily affects magnetic latitudes 55–72°.

[35] In summary, our correlation analysis has shown that EEP is a significant source of mesospheric HO_x at latitudes connected to the outer radiation belt. We have shown that EEP has a measurable effect on OH about 34% of the time. Considering that the time period 2004–2009 analyzed here coincided with an extended minimum of solar activity, and that year 2009 was anomalously quiet with very low radiation belt particle densities, it is reasonable to assume that our results provide a lower-limit estimation of the importance of EEP on HO_x. The electron fluxes and the corresponding OH enhancements are expected to be stronger during the transition from solar maximum to solar minimum.

[36] **Acknowledgments.** M.E.A. would like to thank Marko Laine and Sanna-Mari Päivärinta for helpful comments. M.E.A., C.J.R., and M.A.C. would like to thank the International Space Science Institute (ISSI) of Bern, Switzerland, for providing the environment in which this paper could be completed. The work of M.E.A. and P.T.V. was supported by the Academy of Finland through the projects 136225 and 140888 (SPOC: Significance of Energetic Electron Precipitation to Odd Hydrogen, Ozone, and Climate). Research at the Jet Propulsion Laboratory, California Institute of Technology, is performed under contract with the National Aeronautics and Space Administration. C.J.R. was supported by the New Zealand Marsden Fund.

References

Bates, D. R., and M. Nicolet (1950), The photochemistry of atmospheric water vapor, *J. Geophys. Res.*, *55*, 301–327.

Brasseur, G., and S. Solomon (1986), *Aeronomy of the Middle Atmosphere*, 2nd ed., D. Reidel, Dordrecht, Netherlands.

Canty, T., and K. Minschwaner (2002), Seasonal and solar cycle variability of OH in the middle atmosphere, *J. Geophys. Res.*, *107*(D24), 4737, doi:10.1029/2002JD002278.

Clilverd, M. A., C. J. Rodger, T. Moffat-Griffin, E. Spanswick, P. Breen, F. W. Menk, R. S. Grew, K. Hayashi, and I. R. Mann (2010), Energetic outer radiation belt electron precipitation during recurrent solar activity, *J. Geophys. Res.*, *115*, A08323, doi:10.1029/2009JA015204.

Damiani, A., M. Storini, M. Laurenza, and C. Rafanelli (2008), Solar particle effects on minor components of the Polar atmosphere, *Ann. Geophys.*, *26*, 361–370.

Damiani, A., M. Storini, M. L. Santee, and S. Wang (2010), The hydroxyl radical as an indicator of SEP fluxes in the high-latitude terrestrial atmosphere, *Adv. Space Res.*, *46*, 1225–1235, doi:10.1016/j.asr.2010.06.022.

Evans, D. S., and M. S. Greer (2004), Polar orbiting environmental satellite space environment monitor – 2. Instrument descriptions and archive data documentation, vers. 1.4, *NOAA Tech. Memo. OAR SEC 93*, NOAA, Silver Spring, Md.

Farr, N. L., D. Baker, S. G. Kanekal, and X. Li (2009), A remarkable natural experiment: The extremely quiet Sun (2007–2009) and its effect on Earth's radiation belts, *Eos Trans. AGU*, *90*(52), Fall Meet. Suppl., Abstract SM21B-05.

Frederick, J. E., and R. D. Hudson (1980), Atmospheric opacity in the Schumann-Runge bands and the aeronomic dissociation of water vapor, *J. Atmos. Sci.*, *55*, 301–327.

Gussenhoven, M. S., E. G. Mullen, and D. H. Brautigam (1996), Phillips Laboratory Space Physics Division radiation models, in *Radiation Belts: Models and Standards*, *Geophys. Monogr. Ser.*, vol. 97, edited by J. F. Lemaire, D. Heynderickx, and D. N. Baker, pp. 305–319, AGU, Washington, D. C., doi:10.1029/GM097p0093.

Heaps, M. G. (1978), The effect of a solar proton event on the minor neutral constituents of the summer polar mesosphere, *Tech. Rep. ASL-TR0012*, U.S. Army Atmos. Sci. Lab., White Sands Missile Range, N. M.

Jackman, C. H., et al. (2011), Northern Hemisphere atmospheric influence of the solar proton events and ground level enhancement in January 2005, *Atmos. Chem. Phys.*, *11*, 6153–6166, doi:10.5194/acp-11-6153-2011.

Lam, M. M., R. B. Horne, N. P. Meredith, S. A. Glauert, T. Moffat-Griffin, and J. C. Green (2010), Origin of energetic electron precipitation >30 keV into the atmosphere, *J. Geophys. Res.*, *115*, A00F08, doi:10.1029/2009JA014619.

Lambert, A., et al. (2007), Validation of the Aura Microwave Limb Sounder middle atmosphere water vapor and nitrous oxide measurements, *J. Geophys. Res.*, *112*, D24S36, doi:10.1029/2007JD008724.

Livesey, N. J., et al. (2011), EOS MLS Version 3.3 Level 2 data quality and description document, version 3.3x-1.0, *JPL D-33509*, Jet Propul. Lab., Pasadena, Calif.

Meyer, P., E. N. Parker, and J. A. Simpson (1956), Solar cosmic rays of February 1956 and their propagation through interplanetary space, *Phys. Rev.*, *104*, 768–783.

Millan, R. M., K. B. Yando, J. C. Green, and A. Y. Ukhorskiy (2010), Spatial distribution of relativistic electron precipitation during a radiation belt depletion event, *Geophys. Res. Lett.*, *37*, L20103, doi:10.1029/2010GL044919.

Minschwaner, K., G. L. Manney, S. H. Wang, and R. S. Harwood (2011), Hydroxyl in the stratosphere and mesosphere - Part 1: Diurnal variability, *Atmos. Chem. Phys.*, *11*, 955–962, doi:10.5194/acp-11-955-2011.

Pickett, H. M., W. G. Read, K. K. Lee, and Y. L. Yung (2006), Observation of night OH in the mesosphere, *Geophys. Res. Lett.*, *33*, L19808, doi:10.1029/2006GL026910.

Pickett, H. M., et al. (2008), Validation of Aura Microwave Limb Sounder OH and HO_2 measurements, *J. Geophys. Res.*, *113*, D16S30, doi:10.1029/2007JD008775.

Rodger, C. J., M. A. Clilverd, P. T. Verronen, T. Ulich, M. J. Jarvis, and E. Turunen (2006), Dynamic geomagnetic rigidity cutoff variations during a solar proton event, *J. Geophys. Res.*, *111*, A04222, doi:10.1029/2005JA011395.

Rodger, C. J., M. A. Clilverd, J. C. Green, and M. M. Lam (2010a), Use of POES SEM-2 observations to examine radiation belt dynamics and energetic electron precipitation into the atmosphere, *J. Geophys. Res.*, *115*, A04202, doi:10.1029/2008JA014023.

Rodger, C. J., B. R. Carson, S. A. Cummer, R. J. Gamble, M. A. Clilverd, J.-A. Sauvaud, M. Parrot, J. C. Green, and J.-J. Berthelier (2010b), Contrasting the efficiency of radiation belt losses caused by ducted and non-ducted whistler mode waves from ground-based transmitters, *J. Geophys. Res.*, *115*, A12208, doi:10.1029/2010JA015880.

Schwartz, M. J., et al. (2008), Validation of the aura microwave limb sounder temperature and geopotential height measurements, *J. Geophys. Res.*, *113*, D15S11, doi:10.1029/2007JD008783.

Shapiro, A. V., E. Rozanov, A. I. Shapiro, S. Wang, T. Egorova, W. Schmutz, and T. Peter (2011), Signature of the 27-day solar rotation cycle in mesospheric OH and H_2O observed by the Aura Microwave Limb Sounder, *Atmos. Chem. Phys. Discuss.*, *11*, 28,477–28,498, doi:10.5194/acpd-11-28477-2011.

Sinnhuber, M., S. Kazeminejad, and J. M. Wissing (2011), Interannual variation of NO_x from the lower thermosphere to the upper stratosphere in the years 1991–2005, *J. Geophys. Res.*, *116*, A02312, doi:10.1029/2010JA015825.

Solomon, S., D. W. Rusch, J.-C. Gérard, G. C. Reid, and P. J. Crutzen (1981), The effect of particle precipitation events on the neutral and ion chemistry of the middle atmosphere: II. Odd hydrogen, *Planet. Space Sci.*, *8*, 885–893.

Thorne, R. M. (1977), Energetic radiation belt electron precipitation - A natural depletion mechanism for stratospheric ozone, *Science*, *195*, 287–289.

Turunen, E., P. T. Verronen, A. Seppälä, C. J. Rodger, M. A. Clilverd, J. Tamminen, C.-F. Enell, and T. Ulich (2009), Impact of different precipitation energies on NO_x generation during geomagnetic storms, *J. Atmos. Sol. Terr. Phys.*, *71*, 1176–1189, doi:10.1016/j.jastp.2008.07.005.

Verronen, P. T. (2006), Ionosphere–atmosphere interaction during solar proton events, Ph.D. thesis, University of Helsinki, Helsinki. [Available at http://ethesis.helsinki.fi/julkaisut/mat/fysik/vk/verronen/ionosphe.pdf.]

Verronen, P. T., A. Seppälä, M. A. Clilverd, C. J. Rodger, E. Kyrölä, C.-F. Enell, T. Ulich, and E. Turunen (2005), Diurnal variation of ozone depletion during the October–November 2003 solar proton events, *J. Geophys. Res.*, *110*, A09S32, doi:10.1029/2004JA010932.

Verronen, P. T., A. Seppälä, E. Kyrölä, J. Tamminen, H. M. Pickett, and E. Turunen (2006), Production of odd hydrogen in the mesosphere during the January 2005 solar proton event, *Geophys. Res. Lett.*, *33*, L24811, doi:10.1029/2006GL028115.

Verronen, P. T., C. J. Rodger, M. A. Clilverd, H. M. Pickett, and E. Turunen (2007), Latitudinal extent of the January 2005 solar proton event in the Northern Hemisphere from satellite observations of hydroxyl, *Ann. Geophys.*, *25*, 2203–2215.

Verronen, P. T., C. J. Rodger, M. A. Clivered, and S. Wang (2011), First evidence of mesospheric hydroxyl response to electron precipitation from the radiation belts, *J. Geophys. Res.*, *116*, D07307, doi:10.1029/2010JD014965.

Waters, J. W., et al. (2006), The Earth Observing System Microwave Limb Sounder (EOS MLS) on the Aura Satellite, *IEEE Trans. Geosci. Remote Sens.*, *44*, 1075–1092, doi:10.1109/TGRS.2006.873771.